Computer simulations of colloidal transport on a patterned magnetic substrate

Andrea Fortini and Matthias Schmidt

Theoretische Physik II, Physikalisches Institut, Universität Bayreuth, Universitätsstraße 30, D-95447 Bayreuth, Germany

(Received 20 December 2010; revised manuscript received 4 March 2011; published 29 April 2011)

We study the transport of paramagnetic colloidal particles on a patterned magnetic substrate with kinetic Monte Carlo and Brownian dynamics computer simulations. The planar substrate is decorated with point dipoles in either parallel or zigzag stripe arrangements and exposed to an additional external magnetic field that oscillates in time. For the case of parallel stripes we find that the magnitude and direction of the particle current is controlled by the tilt angle of the external magnetic field. The effect is reliably obtained in a wide range of ratios between temperature and magnetic permeability. Particle transport is achieved only when the period of oscillation of the external field is greater than a critical value. For the case of zigzag stripes a current is obtained using an oscillating external field normal to the substrate. In this case, transport is possible only in the vertex of the zigzag, giving rise to a narrow stream of particles. The magnitude and direction of the particle current are found to be controlled by a combination of the zigzag angle and the distance of the colloids from the substrate. Metropolis Monte Carlo and Brownian dynamics simulations predict results that are in good agreement with each other. Using kinetic Monte Carlo we find that at high density the particle transport is hindered by jamming.

DOI: 10.1103/PhysRevE.83.041411 PACS number(s): 82.70.Dd, 05.10.Ln, 75.75.Jn

I. INTRODUCTION

Manipulation and transport of magnetic particles at the nanometer and micrometer scales are important technological processes for biological [1] and biomedical applications [2]. Magnetic microspheres are routinely used as markers for cells or larger molecules. Micron-sized magnetic beads were attached to the free end of viral DNA [3] for the direct visualization in a bright field microscope of a DNA-packaging process. Molday *et al.* [4] achieved separation of red blood cells and lymphoid cells using magnetic particles chemically bound to antibodies. Pamme and Wilhelm [5] achieved continuous cell sorting of magnetically labeled cells via free-flow magnetophoresis. Magnetic particles can also be tagged with a fluorescent dye and followed in real time using microscopy [6], and their surface can be functionalized to selectively bind to specific targets in a solution, allowing for selective separation using magnetic fields [7].

Since a magnetic particle in a homogenous magnetic field cannot have a net translational motion, a variety of methods have been developed for the generation of inhomogeneous magnetic fields that can be used to manipulate and transport magnetic particles. Deng *et al.* [8] and Lee *et al.* [9] used lithography to fabricate circuits that carry electrical currents in order to generate the inhomogeneous magnetic field that is necessary for manipulating the magnetic particles. Another approach relies on the deposition of discrete ferromagnetic elements. In particular, Yellen *et al.* [10] printed cylindrical magnetic islands on a substrate to drive the assembly of colloidal particles. The application of a rotating external magnetic field allows control and transport of small superparamagnetic particles [11,12]. Gunnarsson *et al.* [13] deposited elliptical magnetic elements and showed the ability to transport paramagnetic particles along the ellipses by the application of a rotating magnetic field. Another technique uses ferrite garnet films [14], which show patterns of alternating magnetization, and an external field that oscillates in time in order to control the transport of colloidal particles [14–17]. The pattern on a garnet film forms spontaneously and is not easily controllable. On the other hand, the deposition of small magnetic islands [10,13] opens up the possibility of creating structured magnetic substrates with full control of the deposition pattern.

In this light, we carry out both kinetic Metropolis Monte Carlo (MC) and Brownian dynamics (BD) computer simulations to study the behavior of paramagnetic colloidal particles on a substrate of discrete magnetic dipoles arranged in two specific patterns, namely parallel and zigzag stripes. The patterns were inspired by those found in garnet films [14–16] but could, in principle, also be fabricated by one of the above deposition techniques [10,13]. The field generated by a garnet film [15] differs quantitatively from the one produced by an array of discrete dipoles. Nevertheless, we show that the differences are small and that our model shows a particle transport behavior similar to the one found experimentally on garnet films. In particular, we find that the random Brownian motion of the colloidal particles is turned into a deterministic motion by an oscillating external magnetic field. We analyze the conditions that enable the deterministic motion and hence the controlled transport of the paramagnetic colloidal particles.

Brownian dynamics is based on the equations of motion for overdamped particles without hydrodynamic interactions; on the other hand, Monte Carlo reproduces the correct dynamics only under certain conditions [18–23]. The advantage of Monte Carlo is its higher computational efficiency with respect to Brownian dynamics. Therefore, we explicitly compare the results of Monte Carlo and Brownian dynamics at low density and carry out only Monte Carlo simulations in the computationally demanding high-density regime.

The paper is organized as follows: In Sec. II we summarize the model used and describe the simulation details. In particular, in Sec. II A we define the particle-particle and particle-substrate interactions; in Sec. II B we discuss the energy landscape of the model, and in Sec. II C we give the simulation details. In Sec. III, we show and discuss the results for both parallel and zigzag stripes. In Sec. IV we give some concluding remarks. In Appendix we discuss similarities and differences between the field produced by our model and that produced by a Garnet film.

II. MODEL AND METHOD

A. Definition of the interactions

We study a fixed lattice of size $N_x \times N_y$ of point magnetic dipoles $\vec{\mathbf{m}}_{ln}$ lying in the x-y plane with components $(\pm m_0,0,0)$. The lattice sites are enumerated by the pair of integers (l,n), where l refers to the x direction and n to the y direction. The x component is $+m_0$ for dipoles sitting at an odd l position and $-m_0$ for dipoles sitting at an even l position. The dipole moments have all the same magnitude m_0 and form a pattern of parallel [Fig. 1(a)] or zigzag stripes [Fig. 1(b)]. The wavelength of the repeating pattern in the x direction is denoted by λ. The separation distance between point dipoles in the y direction is Δy and the separation distance between point dipoles in the x direction is $\Delta x = \lambda/2$. The zigzag pattern is characterized by the angle θ_z, as shown in Fig. 1(b).

The substrate generates a magnetic field

$$\vec{\mathbf{H}}_{\rm sub}(\vec{\mathbf{r}}) = \sum_{l,n} \frac{1}{4\pi}\left[\frac{3\,\vec{\mathbf{r}}_{ln}(\vec{\mathbf{m}}_{ln}\cdot\vec{\mathbf{r}}_{ln})}{r_{ln}^5} - \frac{\vec{\mathbf{m}}_{ln}}{r_{ln}^3}\right], \qquad (1)$$

where $\vec{\mathbf{r}}_{ln}$ is the distance between the dipole (l,n), and the space point $\vec{\mathbf{r}} = (x,y,z)$. In addition, a time-dependent and spatially homogeneous external magnetic field $\vec{\mathbf{H}}_{\rm ext}(t) = \vec{\mathbf{H}}_{\rm ext}^{\rm max}\sin(2\pi t/\tau_0)$ is applied to the system. Here $\vec{\mathbf{H}}_{\rm ext}^{\rm max} = (H^x,H^y,H^z)$ is the amplitude of the external field, τ_0 is its oscillation period, and t is the time.

A colloidal fluid of N paramagnetic spheres with hard-core diameter σ lies suspended at a distance $z_{\rm coll}$ from the patterned substrate and is constrained to move in the x-y plane only. The total magnetic field exerted on a paramagnetic particle i at position $\vec{\mathbf{r}}_i = (x_i,y_i,z_{\rm coll})$ is the sum of the external field and the substrate field

$$\vec{\mathbf{H}}(\vec{\mathbf{r}}_i,t) = \vec{\mathbf{H}}_{\rm sub}(\vec{\mathbf{r}}_i) + \vec{\mathbf{H}}_{\rm ext}(t). \qquad (2)$$

Hence, a dipole moment $\vec{\mathbf{m}}_i = \chi\vec{\mathbf{H}}(\vec{\mathbf{r}}_i,t)$, is induced in the paramagnetic particle i with susceptibility χ.

The interaction energy between the dipoles in the substrate is constant in time, therefore the relevant energy of our model is the sum of three contributions: first, the hard-core interaction between the particles; second, the interaction between the particles' (induced) dipole moments $\vec{\mathbf{m}}_i$ and the total magnetic field $\vec{\mathbf{H}}(x,y,z_{\rm coll},t)$; and, third, the dipole-dipole interaction between the particles. The total energy can therefore be written as

$$\beta U_{\rm tot}(t) = \sum_{i<j}\Phi(r_{ij}) - \beta\mu_s\chi\sum_i \vec{\mathbf{H}}(\vec{\mathbf{r}}_i,t)^2 - \sum_{i<j}\frac{\beta\mu_s\chi^2}{4\pi r_{ij}^3}\Big[3\,\vec{\mathbf{H}}(\vec{\mathbf{r}}_i,t)\cdot\vec{\mathbf{e}}_{ij}\,\vec{\mathbf{H}}(\vec{\mathbf{r}}_j,t)\cdot\vec{\mathbf{e}}_{ij} - \vec{\mathbf{H}}(\vec{\mathbf{r}}_i,t)\cdot\vec{\mathbf{H}}(\vec{\mathbf{r}}_j,t)\Big], \qquad (3)$$

where the hard-sphere potential $\Phi(r_{ij}) = \infty$ if $r_{ij} < \sigma$ and zero otherwise, with $\mathbf{r}_{ij} = |\vec{\mathbf{r}}_i - \vec{\mathbf{r}}_j|$ the distance between colloidal particles i and j, $\vec{\mathbf{e}}_{ij} = \vec{\mathbf{r}}_{ij}/r_{ij}^2$, $\vec{\mathbf{r}}_i = (x_i,y_i,z_{\rm coll})$ and $\vec{\mathbf{r}}_j = (x_j,y_j,z_{\rm coll})$. The field $\vec{\mathbf{H}}$ is defined by Eq. (2), μ_s is the magnetic permeability of the solvent, and $\beta = 1/k_BT$, where k_B is the Boltzmann constant and T is the temperature.

B. Analysis of the energy landscape

As shown by Eq. (3), the particle-particle interaction depends quadratically on χ, while the substrate-particle interaction has a linear dependence on χ. Therefore, in the limit of small χ, the particle-substrate interaction is the leading contribution to the total energy. Hence, valuable information about the model can be extracted by simply analyzing the particle-substrate contribution to the total energy, i.e., the limiting case of a single colloidal particle. The potential (3) for a single particle, taken as $i = 1$, reads $\beta U(x_1,y_1,z_{\rm coll},t) = -\beta\mu_s\chi\vec{\mathbf{H}}(x_1,y_1,z_{\rm coll},t)^2$. Figure 2(a) shows this potential as

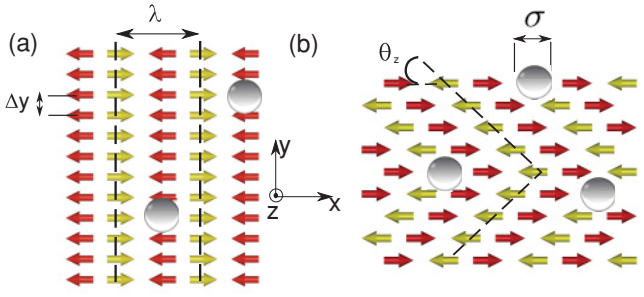

FIG. 1. (Color online) Sketch of the model. The colloidal particles (spheres) are suspended at a distance $z_{\rm coll}$ over a pattern of discrete point dipoles (arrows). The dipoles are oriented along the x axis with alternating magnetization $\vec{\mathbf{m}} = (\pm m_0,0,0)$. The wavelength of the repeating pattern is λ. The particles in the figures are shown with diameter 2σ to help visualization. (a) Parallel stripes pattern. (b) Zigzag pattern with the zigzag angle θ_z as a control parameter.

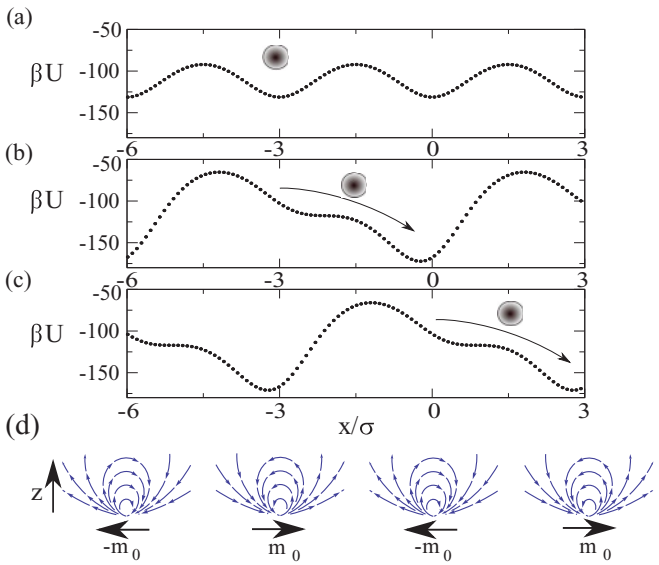

FIG. 2. (Color online) (a) Scaled energy landscape βU as a function of x/σ at position $y = 0$, and $z = z_{\rm coll}$ for a pattern of parallel stripes at time $t = 0$. The circle indicates the preferred position of the particle. (b) Same as (a) but at time $t = \tau_0/4$ in a tilted external potential. The arrow indicates that the particle jumps to the next energy minimum. (c) Same as (b) but at time $t = 3\tau_0/4$. (d) Magnetic field lines of a sequence of positive and negative point dipoles in the x-z plane. These dipoles generate the energy landscape shown in (a).

a function of $x = x_1$ for the case of $y_1 = 0$ and for a pattern of parallel stripes [as shown in Fig. 1(a)], at time $t = 0$. The external field is zero and the energy has a series of minima at the positions of the dipoles [shown in Fig. 2(d)], whereas the maximum of the energy is exactly halfway between two dipoles. Let us assume that at $t = 0$ the particle is sitting in the energy minimum at position $x_1 = -3\sigma$, i.e., at the position of a dipole pointing in the positive direction. At time $t = \tau_0/4$ the external field has positive x and z components. Consequently, it reduces the total field above the dipoles pointing in the positive x direction and enhances the field above the dipoles pointing in the negative x direction. Likewise, the field between dipoles is enhanced and reduced alternately. This gives rise to an asymmetry in the energy landscape, as shown in Fig. 2(b). Due to the presence of a point of inflection in the energy, the particle moves toward the energy minimum that is now located above a negative dipole. At time $t = \tau_0/2$ the external field vanishes, and the energy landscape is the same as shown in Fig. 2(a). On the other hand, at time $t = 3\tau_0/4$ the external field has negative x and z components. The total field above the positive dipoles is now enhanced and the total field above of the negative dipoles is reduced. The field between dipoles is again reduced and enhanced alternately. The point of inflection is again present in the energy landscape [Fig. 2(c)] and the particle moves to the next energy minimum, which is now located above a positive dipole. It is clear from the sequence of Fig. 2 that after one cycle τ_0 of the external field the particle has covered the distance λ and that the cycle can be repeated indefinitely. When the inclination angle of the external field is such that either the z component or the x component is zero, the point of inflection in the energy landscape is never formed and the particle does not move in any preferential direction. For the point of inflection to form both an x and a z component of the external field are necessary to break the symmetry for a pattern of parallel stripes.

The particles can, on average, advance in discrete steps of $0.5\,\lambda$ every half-period τ_0. We will hence quantify the transport by the (time) average current $\langle J_x \rangle = \langle \frac{1}{N} \sum_i \frac{x_i(t) - x_i(t_0)}{t - t_0} \rangle$, where $x_i(t)$ and $x_i(t_0)$ are the positions of the colloidal particle i at time t and initial time t_0, respectively. With this definition, the maximum current measurable is $\langle J_x \rangle = \lambda/\tau_0$, and an average current $\langle J_x \rangle < \lambda/\tau_0$ is an indication of a decreased efficiency of the transport mechanism, e.g., due to thermal motion or collisions among particles. Performing computer simulations, as laid out in the next section, allows us to investigate the values of the external magnetic field that induce a particle current and the effect of the particles' Brownian motion as well as effects due to many particle interactions.

C. Simulation method

The simulation box has a lateral size $L_x \times L_y = 30 \times 60\ \sigma^2$ and has periodic boundary conditions in the x and y directions. The substrate lies in the $z = 0$ plane and contains 2600 point dipoles with dipole moment $m_0 = 50 H_0 \sigma^3$ with H_0 the unit of the magnetic field. We choose a wavelength $\lambda = 3\sigma$ and a dipole separation distance $\Delta y = 0.3\sigma$. The colloidal particles are constrained to move in the $z = z_{\text{coll}} = \text{const.}$ plane and have a susceptibility $\chi = 0.4\,\sigma^3$, arbitrarily chosen such that the linear term in the energy is the leading term. We sampled averages for 100 τ_0, after 5 τ_0 of "equilibration" time. The long-range dipole-dipole interactions are treated through the Ewald sum [24,25]. In order to speed up the interaction calculations, we precompute the field $\vec{\mathbf{H}}_{\text{sub}}$ due to the substrate on a 400×400 grid. During the simulations, the field intensity is obtained by interpolation of the tabulated values. The time is in units of the Brownian time $\tau_B = \sigma^2/D$, with $D = k_B T/\xi$ the Stokes-Einstein diffusion coefficient of the particles and ξ the friction coefficient of the solvent. In our simulations, the hydrodynamic interactions are neglected. Due to solvent hydrodynamics, the diffusion coefficient of particles depends on their distance from the substrate [26–33]. Therefore, simulation carried out at constant distance z_{coll} are characterized by a Brownian time τ_B that depends on z_{coll}. However, this has no effects on our results because they are scaled by the Brownian time. Further many-body effects due to hydrodynamics are neglected, though.

We carry out both standard Metropolis MC [34] simulations with a small MC displacement, $d = 0.01\sigma$, and BD simulations [34]. The relationship between MC and BD has been extensively studied in the literature. Both modified MC schemes [18–20] as well as standard Metropolis MC simulations [21–23] give dynamical properties that can be in good agreement with the results of BD simulations. In particular, it was recently shown [23] that the dynamical properties obtained from Metropolis MC simulations are in good agreement with those obtained from BD as long as the maximum step size of the MC move, d, is small enough and the time scale in MC simulations is obtained according to the relations $\delta t = a d^2/6\,\tau_B$, where a is the average acceptance probability of the MC moves. The relation was demonstrated for one particle in a arbitrary one-dimensional potential and verified explicitly for a many-body system and various three-dimensional potentials. Scaling the time with the acceptance probability in equivalent to advancing the MC time only when a move is accepted, this concept was called "internal clock" by Royall *et al.* [35]. Given the presence of an oscillating external field in our model we explicitly investigate the agreement between MC and BD simulations at low particle density.

We carried out simulations for a set of four distances between the colloidal particles and the substrates, $z_{\text{coll}} = 1.0, 1.5, 1.7, 2\,\sigma$. For $z_{\text{coll}} = 1.0\,\sigma$ the current $\langle J_x \rangle$ was zero in all cases while the results for $z_{\text{coll}} = 1.5, 1.7, 2\,\sigma$ are discussed in detail below.

III. RESULTS

First we study the low-density behavior of the suspended fluid of colloidal particles on a pattern of parallel lines of point dipoles, as shown in Fig. 1(a). We apply a tilted oscillating external magnetic field, with vanishing y component, $H^y_{\text{ext}}(t) = 0$, and x and z components given by $H^{x,z}_{\text{ext}}(t) = H^{x,z} \sin(2\pi t/\tau_0)$. The current measurements were conducted using only a single colloidal particle. Figure 3(a) shows the time average current $\langle J_x \rangle$ as a function of the oscillation period of the external field $\vec{\mathbf{H}}_{\text{ext}}(t)$ for three different values of z_{coll} and with $k_B T/\mu_s = 5 \times 10^{-3}$. We find that the current is induced only for values of the oscillation period τ_0 larger than a critical value. This result can be interpreted easily. If the external magnetic field is oscillating too quickly (small

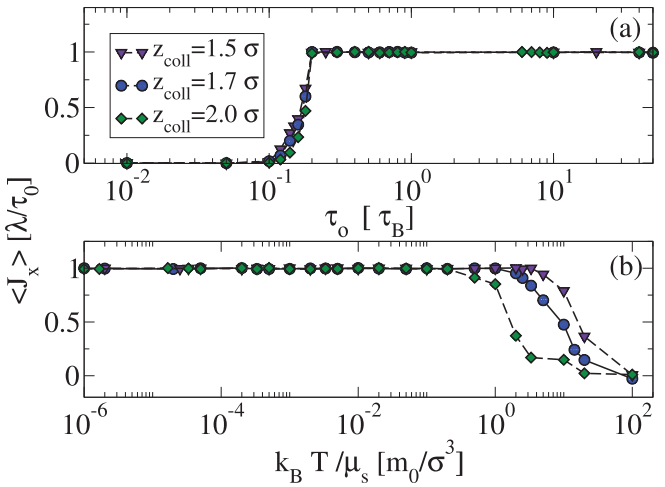

FIG. 3. (Color online) Average current $\langle J_x \rangle$ in the direction perpendicular to the parallel stripes for $z_{\rm coll} = 1.5, 1.7, 2.0\,\sigma$. (a) As a function of the period τ_0 of the external field. (b) As a function of the temperature-susceptibility ratio, $k_B T/\mu_s$, with an external field oscillation period $\tau_0 = 10\tau_B$.

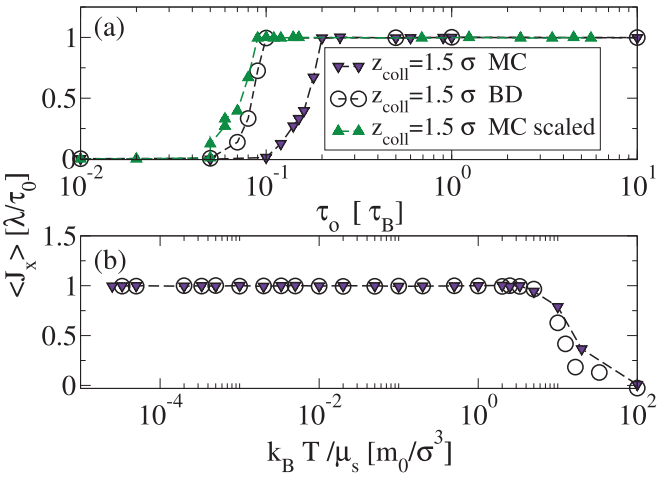

FIG. 4. (Color online) Comparison among MC, MC scaled with the acceptance probability a, and BD simulation results for the measured average current $\langle J_x \rangle$ for $z_{\rm coll} = 1.5\,\sigma$. (a) As a function of the period τ_0 of the external field. (b) As a function of the temperature-susceptibility ratio, $k_B T/\mu_s$, with an external field oscillation period $\tau_0 = 10\tau_B$.

period, high frequency) on the scale of the characteristic diffusion time (Brownian time), then the particle is unable to follow the rapidly changing energy landscape. Figure 3(b) shows the x component of the measured current $\langle J_x \rangle$, as a function of $k_B T/\mu_s$, for three different values of $z_{\rm coll}$ and with $\tau_0 = 100\tau_B$.

We find that the external field drives a particle current for values of temperature over permeability, $k_B T/\mu_s$ smaller than a critical value. This result suggests that if the thermal energy is too large, the Brownian motion randomizes the motion of the colloidal particles and suppresses the transport.

Figure 4(a) shows the comparison between MC and BD simulation results for the current as a function of the period of oscillation τ_0. The two simulation techniques give qualitatively the same behavior, including the presence of a critical oscillation period beyond which the transport is possible. Nevertheless, the BD predicts a critical period that is 2 times smaller than that of the MC simulations. We also show the period rescaled by the average acceptance probability a as suggested by Sanz and Marenduzzo [23]. The procedure leads to a much better (but not perfect) comparison. On the other hand, for oscillation periods far from the critical value, the comparison between BD and MC is very good. Figure 4(b) shows that for a value $\tau_0 = 10\tau_B$, both BD and MC simulations give the same behavior for the current as a function of the temperature over permeability.

Figure 5(a) shows the value of the average current $\langle J_x \rangle$ as a function of the magnitude of the external field $|H_{\rm ext}|$, at a fixed inclination angle $\theta_t = \arctan(H^y/H^x) = 45^\circ$ of the external magnetic field, $z_{\rm coll} = 1.7\sigma$, and with an oscillation period $\tau_0 = 10\tau_B$. We find that a critical value of the external field needs to be reached in order to initiate the particle transport. Figure 5(b) shows the value of the average current $\langle J_x \rangle$ as a function of the inclination angle θ_t at a fixed external field magnitude $|H_{\rm ext}|$ and for $z_{\rm coll} = 1.7\,\sigma$. We find that the current magnitude and direction can both be controlled by the inclination angle of the external magnetic field. Note that for angles $\theta_t = \pm 180^\circ, \pm 90^\circ, 0^\circ$ the current is zero. These angles correspond to an external field with either only a component of the external magnetic field parallel to the substrate ($\theta_t = \pm 180^\circ, 0^\circ$) or only a component normal to the substrate ($\theta_t = \pm 90^\circ$). Figure 5 also shows BD simulation results. The comparison between MC and BD simulations is very good.

We next investigate the dependence on particle density. We characterize the system by a linear density $\rho = 2\sigma N/N_x L_y$, where N is the total number of particles. Here, we carried out only MC simulations. These posses higher computational efficiency over BD at the large number of particles that we are considering. Figure 6 shows the current induced on a parallel stripes pattern as a function of ρ. We find that the

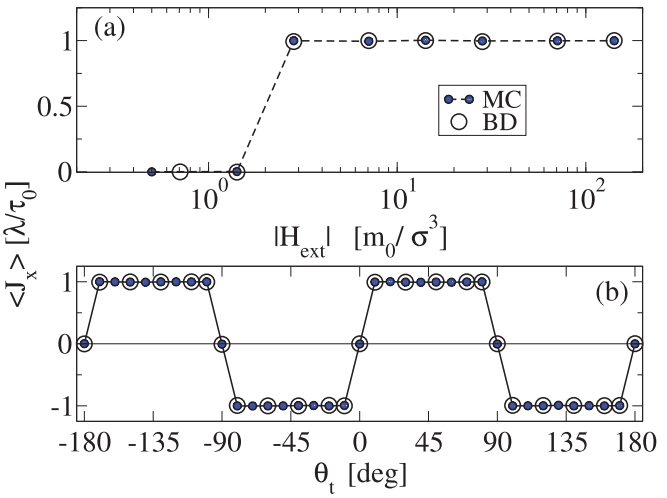

FIG. 5. (Color online) Average current $\langle J_x \rangle$ in the direction perpendicular to the parallel stripes for $z_{\rm coll} = 1.7\,\sigma$. (a) As a function of the magnitude $|H_{\rm ext}|$ of the external field at an inclination angle $\theta_t = \arctan(H^y/H^x) = 45^\circ$. (b) As a function of the inclination angle θ_t for a magnitude $|H_{\rm ext}| = 50\, m_0/\sigma^3$.

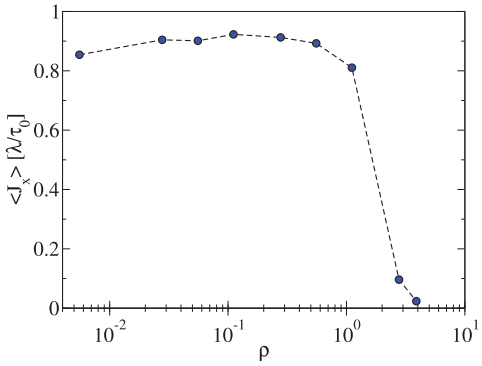

FIG. 6. (Color online) Average current $\langle J_x \rangle$ for a pattern of parallel stripes, $z_{\rm coll} = 1.7\,\sigma$, $\tau_0 = 10\tau_B$, and $k_BT/\mu_s = 0.05$ as a function of the linear density ρ.

current remains roughly constant at low densities with a value slightly smaller than unity. This result indicates a decreased efficiency of the transport mechanism due to the presence of other particles. Interestingly, the current decays to zero at densities larger than $\rho \simeq 2$. At this density, all stripes are filled with particles. If more particles are present, they must fill positions that are not ideal for the transport mechanism. These excess particles effectively jam the transport.

We next analyze the motion of the particles suspended over a zigzag pattern with an external field perpendicular to the substrate. The x and y components of the external field vanish, $H_{\rm ext}^{x,y}(t) = 0$, and the perpendicular z component, $H_{\rm ext}^{z}(t) = H^z \sin(2\pi t/\tau_0)$, is oscillating in time with period τ_0. Analysis of the particles trajectories shows that transport is achievable only in the vertex region of the zigzag. Therefore, to reliably measure the current, we initialized the simulations with a single colloid randomly positioned along the x direction but localized at the vertex. Figure 7(a) shows the current $\langle J_x \rangle$ as a function of the period of oscillation τ_0 for three different values of $z_{\rm coll}$ and for $\theta_z = 68^\circ$. As for the case of parallel lines, the period of oscillation of the external field needs to be large enough in order to induce a current. Furthermore, we

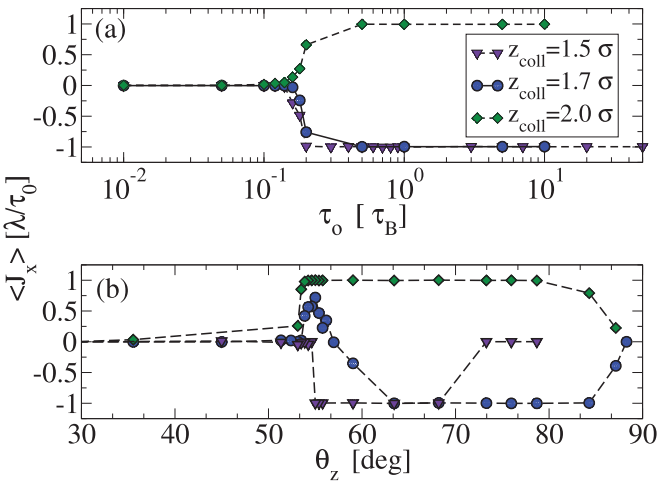

FIG. 7. (Color online) Average current $\langle J_x \rangle$ for a zigzag pattern with $k_BT/\mu_s = 5 \times 10^{-3}$ for $z_{\rm coll} = 1.5, 1.7, 2.0\sigma$. (a) As a function of the oscillation period τ_0 of the external field for $\theta_z = 68^\circ$. (b) As a function of the zigzag angle θ_z for $\tau_0 = 7\tau_B$.

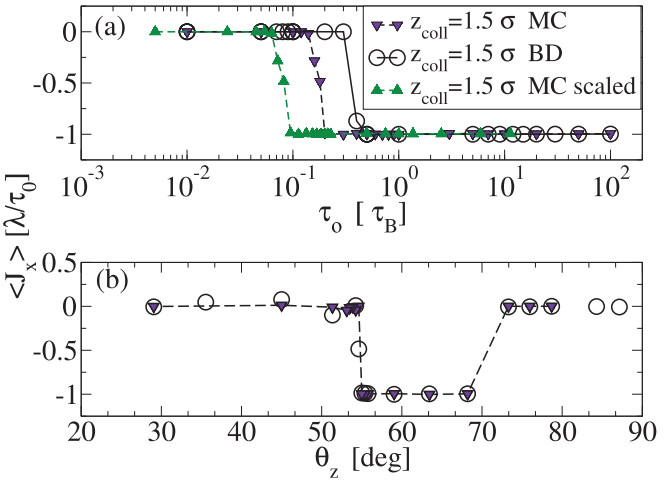

FIG. 8. (Color online) Comparison among MC, MC scaled with the acceptance probability a, and BD simulation for the measured average current $\langle J_x \rangle$ for $z_{\rm coll} = 1.5\sigma$. (a) As a function of the oscillation period τ_0 of the external field for $\theta_z = 68^\circ$. (b) As a function of the zigzag angle θ_z for $\tau_0 = 7\tau_B$.

find that for $z_{\rm coll} = 1.5, 1.7\sigma$ the current is negative, whereas for $z_{\rm coll} = 2.0\sigma$ the current is positive. Figure 7(b) shows the average current as a function of the zigzag angle θ_z for external field $H_z = 10\ m_0/\sigma^3$ and $\tau_0 = 100\tau_B$. The current direction differs for different distances $z_{\rm coll}$. In particular, it is positive for $z_{\rm coll} = 2.0\sigma$ and negative for $z_{\rm coll} = 1.5\sigma$. Interestingly, for the intermediate value $z_{\rm coll} = 1.7\sigma$, the current is negative for large angles but positive at smaller zigzag angles. The current vanishes for $\theta_z = 90^\circ$, corresponding to the case of parallel stripes. We stress that the current is obtained only at the zigzag vertex because the external field only has a normal component. This means that the local relative position of the dipole located around the vertex plays a fundamental role in the creation of the point of inflection in the energy that is necessary for the transport mechanism (see Sec. II B). Nevertheless, if a tilted external field is applied to the zigzag patterns, transport is achieved also away from the vertex. Figures 8(a) and 8(b) show the comparison between MC and BD simulations for $z_{\rm coll} = 1.5\sigma$. We find a discrepancy in the predicted value of the critical period. Contrary to the case of the parallel lines pattern, the BD predicts a critical period that is 2 times larger than MC. Rescaling with the average acceptance probability leads to a worse comparison. On the other hand, the comparison is very good for the current as a function of the zigzag angle for a value of the oscillation period $\tau_0 = 7\tau_B$ far from the critical value.

IV. CONCLUSIONS

We have studied a simple model for the transport of colloidal particles suspended at a fixed distance over a magnetic patterned substrate with MC and BD computer simulations Magnetic dipoles were distributed in two specific patterns, namely parallel stripes and zigzag stripes. We analyzed the effect of an oscillating external magnetic field that was applied to the system.

For the case of parallel stripes we found that the current magnitude and direction was controlled by the tilt angle of the

external field and that the effect was reliably obtained in a wide range of ratios between temperature and solvent permeability. Furthermore, a net current was measured only when the period of oscillation was greater than a critical value. For the case of zigzag stripes a current was obtained using an oscillating external field normal to the substrate. In this case, transport was possible only in a small region of the patterned substrate, namely near the vertex of the zigzag. This result opens up the possibility to transport colloidal particles in a very narrow stream. Furthermore, the current magnitude and direction was found to be controlled by a combination of the zigzag angle and the distance of the colloids from the substrate. The comparison between MC and BD is overall qualitatively very good. We find quantitative agreement for values of the period of oscillation of the external field far from the critical period, while the two simulations techniques predicts quantitatively different values of the critical period beyond which transport of particles is possible.

The mechanism behind the transport of the colloidal particles is a consequence of the changing energy landscape. The sum of the oscillating external field and of the substrate's magnetic field results in an energy landscape that changes in time. The Brownian motion enables the particles to locally sample the phase space and follow the energy landscape toward the local (in space and time) energy minimum. Colloidal transport is hence achieved when the particles are able to "follow" this landscape. The mechanism explained here is the same as the one described by Dhar *et al.* [14] as a deterministic ratchet. Yellen *et al.* [11] found the same mechanism and describe it as particles following a traveling wave. That is, the particle is transported by the translating inflection point in the energy landscape. We find that transport of the paramagnetic colloidal particles is possible for a large set of model parameters. The magnetic patterns can be created by deposition of discrete magnetic islands [10–12]. Despite that the field generated by a garnet film [15] differs quantitatively from the one produced by an array of discrete dipoles, the differences are surprisingly small (see Appendix). Therefore, we expect that the behavior for the transport of particles on top of garnet films is similar to the one shown by our model.

Controlling the deposition pattern means controlling the behavior of the nano or micro magnetic particles. As a consequence laboratory-on-chip devices with well-defined functions can be envisioned. Our model and method can be easily applied to different and more complicated patterns, like, for example, a combination of parallel and zigzag stripes. Other possible extensions of the current work include the study of substrate boundary effects. In this work we applied periodic boundary condition, but it would be interesting to study the transport of colloidal particles on top of finite discrete patterns.

Furthermore, given the range of phenomena shown by two-dimensional colloidal suspensions of paramagnetic particles trapped at a liquid-air interface (see, for example, Ebert *et al.* [36] and references therein) it would be interesting to explore in more detail the effect of a patterned magnetic substrate on the phase behavior and the dynamical properties of two-dimensional fluids.

ACKNOWLEDGMENTS

We thank Thomas M. Fischer and Saeedeh Aliaskarisohi for useful discussions and acknowledge the DFG for support via SFB840/A3.

APPENDIX: GARNET FILM

Tierno *et al.* [15] calculated the magnetic field above the garnet film, for a pattern of parallel stripes aligned in the y direction as $\vec{\mathbf{H}} = \nabla \mathrm{Re}[\Phi]$ with the potential

$$\Phi = \frac{i}{\pi}\mathrm{dilog}\left\{1-\exp\left[\frac{4i\pi}{2}w+\mathrm{Im}(h)\right]\right\} - \frac{i}{\pi}\mathrm{dilog}\left\{1+\exp\left[\frac{4i\pi}{2}w-\mathrm{Im}(h)\right]\right\}, \tag{A1}$$

with $w = x + iz$ and $h = \vec{\mathbf{H}}_{\mathrm{ext}} \cdot (\vec{\mathbf{e}}_x - i\vec{\mathbf{e}}_z)$ and the dilogarithm function $\mathrm{dilog}(t) = \int_1^z dt \frac{\ln(t)}{(1-t)}$. Figure 9 shows the comparison between the energy of the garnet film from the potential (A1) and the energy of an array of dipoles from Eq. (3). The energies were shifted by the mean value $\langle E \rangle$ and rescaled by the maximum value of the energy $E_{\max}$. Both with and without external field the differences between the two energies are small, validating the use of the set of discrete dipoles as a good approximation for patterns on garnet films.

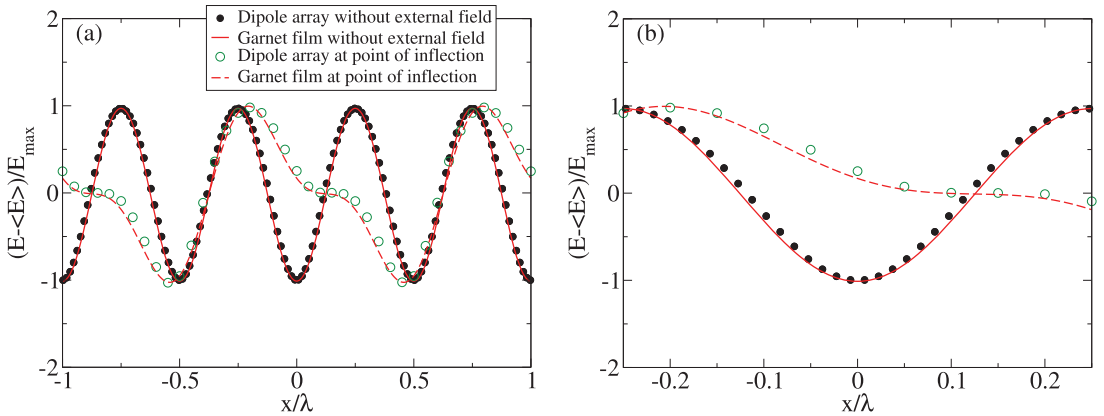

FIG. 9. (Color online) (a) Comparison between the energy of one paramagnetic particle in the magnetic field of a garnet film and the dipole array. (b) Like (a) but zoomed in to highlight the differences.

[1] C. Thomas, Z. Zhang, and C. Cowen, Biotechnol. Lett. **22**, 531 (2000).
[2] J. Fisher, J. Cummings, K. Desai, L. Vicci, B. Wilde, K. Keller, C. Weigle, G. Bishop, R. Taylor, and C. Davis, Rev. Sci. Instrum. **76**, 053711 (2005).
[3] C.-L. Chang, H. Zhang, D. Shu, P. Guo, and C. A. Savran, Appl. Phys. Lett. **93**, 153902 (2008).
[4] R. S. Molday, S. P. S. Yen, and A. Rembaum, Nature **268**, 437 (1977).
[5] N. Pamme and C. Wilhelm, Lab Chip **6**, 974 (2006).
[6] J. Gao, W. Zhang, P. Huang, B. Zhang, X. Zhang, and B. Xu, J. Am. Chem. Soc. **130**, 3710 (2008).
[7] J. T. Kemshead and J. Ugelstad, Mol. Cell. Biochem. **67**, 11 (1985).
[8] T. Deng, G. Whitesides, M. Radhakrishnan, G. Zabow, and M. Prentiss, Appl. Phys. Lett. **78**, 1775 (2001).
[9] C. Lee, H. Lee, and R. Westervelt, Appl. Phys. Lett. **79**, 3308 (2001).
[10] B. B. Yellen, G. Friedman, and A. Feinerman, J. Appl. Phys. **93**, 7331 (2003).
[11] B. B. Yellen, R. M. Erb, H. S. Son, R. Hewlin, H. Shang, and G. U. Lee, Lab Chip **7**, 1681 (2007).
[12] B. B. Yellen and L. N. Virgin, Phys. Rev. E **80**, 011402 (2009).
[13] K. Gunnarsson, P. Roy, S. Felton, J. Pihl, P. Svedlindh, S. Berner, H. Lidbaum, and S. Oscarsson, Adv. Mater. **17**, 1730 (2005).
[14] P. Dhar, P. Tierno, J. Hare, T. Johansen, and T. M. Fischer, J. Phys. Chem. B **111**, 13097 (2007).
[15] P. Tierno, S. V. Reddy, T. H. Johansen, and T. M. Fischer, Phys. Rev. E **75**, 041404 (2007).
[16] P. Tierno, S. V. Reddy, M. G. Roper, T. H. Johansen, and T. M. Fischer, J. Phys. Chem. B **112**, 3833 (2008).
[17] S. Aliaskarisohi, T. H. Johansen, and T. M. Fischer, J. Phys. Chem. B **115**, 2243 (2011)
[18] M. J. Kotelyanskii and U. W. Suter, J. Chem. Phys. **96**, 5383 (1991).
[19] D. M. Heyes and A. C. Branka, Mol. Phys. **94**, 447 (1998).
[20] X. Z. Cheng, M. B. A. Jalil, H. K. Lee, and Y. Okabe, Phys. Rev. Lett. **96**, 067208 (2006).
[21] K. Kikuchi, M. Yoshida, T. Maekawa, and H. Watamabe, Chem. Phys. Lett. **185**, 335 (1991).
[22] L. Berthier, G. Biroli, J.-P. Bouchaud, W. Kob, K. Miyazaki, and D. R. Reichman, J. Chem. Phys. **126**, 184503 (2007).
[23] E. Sanz and D. Marenduzzo, J. Chem. Phys. **132**, 194102 (2010).
[24] P. P. Ewald, Ann. Phys. **64**, 253 (1921).
[25] A. Grzybowski and A. Brodka, Chem. Phys. Lett. **361**, 329 (2002).
[26] K. Zahn, J. M. Mendez-Alcaraz, and G. Maret, Phys. Rev. Lett. **79**, 175 (1997).
[27] O. Reynolds, Philos. Trans. R. Soc. London **177**, 157 (1886).
[28] A. Goldman, R. G. Cox, and H. Brenner, Chem. Eng. Sci. **22**, 637 (1967).
[29] J. Klein and E. Kumacheva, J. Chem. Phys. **108**, 6996 (1998).
[30] H. Diamant, J. Phys. Soc. Jpn. **78**, 041002 (2009).
[31] B. Cui, H. Diamant, B. Lin, and S. A. Rice, Phys. Rev. Lett. **92**, 258301 (2004).
[32] F. Benmouna and D. Johannsmann, J. Phys. Condens. Matter **15**, 3003 (2003).
[33] F. Benmouna and D. Johannsmann, Eur. Phys. J. E **9**, 435 (2002).
[34] M. P. Allen and D. J. Tildesley, *Computer Simulation of Liquids* (Oxford University Press, Oxford, 1987).
[35] C. P. Royall, J. Dzubiella, M. Schmidt, and A. van Blaaderen, Phys. Rev. Lett. **98**, 188304 (2007).
[36] F. Ebert P. Dillmann, G. Maret, and P. Keim, Rev. Sci. Inst. **80**, 083902 (2009).